# Comparison of Characteristic Structural Features among the Triade of Tris(cyclopentadienyl)(Group-4 Metal) Complex Cations: a Combined Theoretical and Experimental Study[1])

by **Heiko Jacobsen**[a]), **Heinz Berke**[a])*, **Thomas Brackemeyer**[b]), **Tanja Eisenblätter**[b]), **Gerhard Erker**[b])*, **Roland Fröhlich**[b]), **Oliver Meyer**[b]), and **Klaus Bergander**[b])

[a]) Anorganisch-chemisches Institut, Universität Zürich-Irchel, Winterthurerstr. 190, CH-8057 Zürich
[b]) Organisch-Chemisches Institut, Universität Münster, Corrensstrasse 40, D-48149 Münster

A density functional theory computational chemistry study has revealed a fundamental structural difference between $[Ti(Cp)_3]^+$ and its congeners $[Zr(Cp)_3]^+$ and $[Hf(Cp)_3]^+$/(Cp = cyclopentadienyl). Whereas the latter two are found to contain three uniformely $\eta^5$-coordinated Cp ligands ($3\eta^5$-structural type), $[Ti(Cp)_3]^+$ is shown to prefer a $2\eta^5\eta^2$ structure. $[Ti(Cp)_3]^+[B(C_6F_5)_3(Me)]^-$ (**10**·$[B(C_6F_5)_3(Me)]^-$) was experimentally generated by treatment of $[Ti(Cp)_3(Me)]$ (**7a**) with $B(C_6F_5)_3$ (*Scheme 3*). Low-temperature $^1$H-NMR spectroscopy in $CDFCl_2$ (143 K, 600 MHz; *Fig. 8*) showed a splitting of the Cp resonance into five lines in a 2 : 5 : 2 : 5 : 1 ratio which would be in accord with the theoretically predicted $2\eta^5\eta^2$-type structure of $[Ti(Cp)_3]^+$. The precursor $[Ti(Cp)_3(Me)]$ (**7a**) exhibits two $^1$H-NMR Cp resonances in a 10 : 5 ratio in $CD_2Cl_2$ at 223 K. Treatment of $[HfCl(Cp)_2(Me)]$ (**6c**) with sodium cyclopentadienide gave $[Hf(Cp)_3(Me)]$ (**7c**) (*Scheme 1*). Its reaction with $B(C_6F_5)_3$ furnished the salt $[Hf(Cp)_3]^+[B(C_6F_5)_3(Me)]^-$ (**8**·$[B(C_6F_5)_3(Me)]^-$), which reacted with *tert*-butyl isocyanide to give the cationic complex $[Hf(Cp)_3(C{\equiv}N{-}CMe_3)]^+$ (**9a**; with counterion $[B(C_6F_5)_3(Me)]^-$ (*Scheme 2*). Complex cation **9a** was characterized by X-ray diffraction (*Fig. 7*). Its $Hf(Cp_3)$ moiety is of the $3\eta^5$-type. The structure is distorted trigonal-pyramidal with an average D–Hf–D angle of 118.8° and an average D–Hf–C(1) angle of 96.5° (D denotes the centroids of the Cp rings; *Table 6*). Cation **9a** is a typical $d^0$-isocyanide complex exhibiting structural parameters of the $C{\equiv}N{-}CMe_3$ group ($d(C(1){-}N(2)) =$ 1.146(5) Å; IR: $\tilde{\nu}(C{\equiv}N)$ 2211 $cm^{-1}$) very similar to free uncomplexed isonitrile. Analogous treatment of **8** with carbon monoxide yielded the carbonyl ($d^0$-group-4-metal) complex $[Hf(Cp)_3(CO)]^+$ (**9b**; with counterion $[B(C_6F_5)_3(Me)]^-$) (*Scheme 2*) that was also characterized by X-ray crystal-structure analysis (*Fig. 6*). Complex **9b** is also of the $3\eta^5$-structural type, similar to the peviously described cationic complex $[Zr(Cp)_3(CO)]^+$, and exhibits properties of the CO ligand ($d(C{-}O) = 1.11(2)$ Å; IR: $\tilde{\nu}(C{\equiv}O)$ 2137 $cm^{-1}$) very similar to the free carbon monoxide molecule.

**1. Introduction.** – Tetrakis(cyclopentadienyl)zirconium ($[Zr(Cp)_4]$; **1b**) possesses a solid state structure that is characterized by the presence of three $\eta^5$-cyclopentadienyl ($\eta^5$-Cp) ligands and a single $\sigma$-bonded, *i.e.*, $\eta^1$-coordinated, Cp group [1]. The resulting $3\eta^5\eta^1$-type structure would formally imply a 20-electron configuration to be associated with the central d-block metal, but since the theoretical analysis carried out by *Lauher* and *Hoffmann* [2], and subsequently by *Bursten et al.* [3], it is known that these complexes contain a doubly occupied HOMO that is largely, if not exclusively, ligand-centered. In this way, an unfavorable electronic configuration at the early transition-metal center is very effectively circumvented.

Nevertheless, structures that contain the $[M(\eta^5\text{-}Cp)_3]$ building block ($3\eta^5$-type) are not necessarily always favored over their lower-hapticity alternatives. This became

[1]) Theoretical work was carried out at the Universität Zürich, experimental work at the Universität Münster.

evident when detailed structure analyses of the complete group-4 $[M(Cp)_4]$ triade had become available: both the corresponding titanium and hafnium congeners exhibit the alternative $2\eta^5 2\eta^1$-type structures, *i.e.*, they appear as $[M(\eta^5\text{-}Cp)_2(\eta^1\text{-}Cp)_2]$ (M=Ti (**1a**) and Hf (**1c**)) systems, as shown for both by X-ray structure analyses and, in addition for **1a** by dynamic NMR spectroscopy [4][5] (see *Fig. 1*). In contrast, both $[Zr(Cp)_3H]$ (**1d**) and $[Hf(Cp)_3H]$ (**1e**) seem to have analogous $3\eta^5$-type structures, as evidenced by IR/*Raman* spectroscopy [6]. The zirconium(III) system $[Zr(Cp)_3]$ (**2b**) has been shown to exhibit a $3\eta^5$ structure (determined by X-ray diffraction) [7], whereas the related complex $[ZrBr\{1,3\text{-}(t\text{-}Bu)_2C_5H_3\}(Cp)_2]$ (**1f**) has its bulky substituted cyclopentadienyl ligand slipped to the $\eta^2$-bonding mode [8]. The analogous $2\eta^5\eta^2$-type structure was also established by X-ray diffraction for the paramagnetic complex $[Ti(Cp)_3]$ (**2a**) [9].

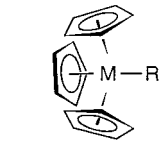


$3\eta^5$
**1b** M = Zr, R = $\eta^1$-Cp
**d** M = Zr, R = H
**e** M = Hf, R = H

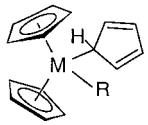


$2\eta^5,\eta^1$
**1a** M = Ti, R = $\eta^1$-Cp
**c** M = Hf, R = $\eta^2$-Cp

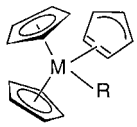


$2\eta^5,\eta^2$
**1f** M = Zr, R = Br
($\eta^2$-ligand substituted)

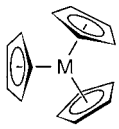


$3\eta^5$
**2b** M = Zr

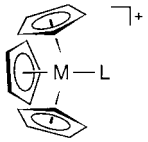


$3\eta^5$
**3a** M = Zr, L = $[B(C_6F_5)_3(Me)]^-$(ion pair)
**b** M = Zr, L = THF
**c** M = Zr, L = CO
**d** M = Zr, L = N≡CMe
**e** M = Zr, L = CN≡$CMe_3$

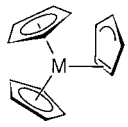


$2\eta^5,\eta^2$
**2a** M = Ti

Fig. 1. *Schematic representation of observed structural types of group-4 metal complexes containing [M(Cp)$_3$] moieties*

We have recently prepared a series of cationic tris(cyclopentadienyl)zirconium complexes. The ion pair $[Zr(Cp)_3]^+[B(C_6F_5)_3(Me)]^-$ (**3a**) and also the corresponding THF adduct $[Zr(Cp)_3(THF)]^+$ (**3b**) appear to have $3\eta^5$-type structures according to their spectroscopic features. The complexes $[Zr(Cp)_3(L)]^+$ **3c** (L = CO), **3d** (L = N≡C–Me), and **3e** (L = C≡$NCMe_3$) were shown by X-ray crystal-structure analyses to adopt $3\eta^5$ structures in the solid state [10] (*Fig. 1*).

In view of the structural dichotomy of the corresponding triads of $[M(Cp)_4]$, $[M(Cp)_3(R)]$, and $[M(Cp)_3]$ titanium, zirconium, and hafnium complexes, it was not *a priori* evident, which of the possible structural types would be favored for the corresponding cationic $[M(Cp)_3(L)]^+$ systems. In this study, we tried to answer this

question experimentally for a pair of related $[Hf(Cp)_3(L)]^+$ systems which were synthesized and characterized by X-ray crystal-structure analyses. We also obtained spectroscopic evidence about the structural properties of a related $[Ti(Cp)_3]^+$ system and a relevant precursor and secured these findings by an independent supporting computational-chemistry study. Together, this revealed a comprehensive picture of the structural preferences of such cationic tris(cyclopentadienyl)metal complexes in the group-4 metal series titanium, zirconium, and hafnium.

**2. Results and Discussion.** – 2.1. *Theoretical Studies. General*. The examination of the structures of the cationic $d^0$ complexes $[M(Cp)_3]^+$ (M = Ti, Zr, Hf) constitutes the starting point of our theoretical investigation. These compounds are isoelectronic to the corresponding neutral group-3 systems, for which a variety of structures have been characterized by X-ray diffraction methods [11]. For the sake of comparison, we also include the $d^1$ species $[M(Cp)_3]$ (M = Ti, Zr, Hf) in our study. We then extend our analysis to the cationic donor-ligand complexes $[M(Cp)_3(L)]^+$ (L = CO, CNMe, NCMe). We want to estimate the relative stabilities of the different M–L linkages, and to elucidate the nature of this particular chemical bond. Our study is based on density functional theory (DFT) [12], and we will frequently use an energy decomposition scheme in our discussion. We will begin with a concise description of our approach toward bonding analysis; a more detailed account will be presented in the *Sect. 3* (computational methods) of the *Exper. Part.*

*Energy Analysis.* The binding energy *BE*, which is associated with the formation of a molecule from appropriate fragments, can be broken down into three major components [13] (*Eqn. 1*). When building up the chemical bond, the fragments are first placed at their positions in the molecule. This implies an electrostatic *Coulomb* interaction $\Delta E_{elstat}$. The term $\Delta E_{Pauli}$, which is called exchange repulsion or *Pauli* repulsion, takes into account the destabilizing two-orbital four-electron interactions between occupied orbitals. The third term on the right hand side of *Eqn. 1*, $\Delta E_{int}$, introduces the attractive orbital interactions. The terms $\Delta E_{elstat}$ and $\Delta E_{Pauli}$ are often combined to the so-called steric interaction term $\Delta E^0$ (*Eqn. 2*).

$$BE = -[\Delta E_{elstat} + \Delta E_{Pauli} + \Delta E_{int}] \quad (1)$$

$$\Delta E^0 = \Delta E_{elstat} + \Delta E_{Pauli} \quad (2)$$

*Possible Structures of $[M(Cp)_3]^+$ Fragments.* Several $2\eta^5\eta^x$ ($x = 1,2,3,5$) isomers of $[M(Cp)_3]^+$ were considered as likely candidates for local-minimum geometries. These studies were performed for $[Zr(Cp)_3]^+$ as an exemplary case. The structures of $3\eta^5$-$[Zr(Cp)_3]^+$ and $2\eta^5\eta^2$-$[Zr(Cp)_3]^+$ could be identified as local minima on the potential-energy surface. The latter one is isoelectronic to $[Zr(\eta^3\text{-allyl})(\eta^4\text{-butadiene})(\eta^5\text{-Cp})]$, for which the electronic structure has already been analyzed using extended-*Hückel* methods [14]. Attempts to optimize structures with $2\eta^5\eta^1$ and $2\eta^5\eta^3$-coordination geometries were not successful; the starting geometries converged to the isomers $2\eta^5\eta^2$-$[Zr(Cp)_3]^+$ and $3\eta^5$-$[Zr(Cp)_3]^+$, respectively.

The structures of the two $[Zr(Cp)_3]^+$ complexes as representative examples for $3\eta^5$ and $2\eta^5\eta^2$ isomers are displayed in *Fig. 2*. For the $3\eta^5$-coordinated molecule, the isomer

of $C_{3h}$ symmetry is shown[2]). This also corresponds to the local coordination mode around the Zr-center as found in the crystal structure of the neutral system $[Zr(Cp)_3]$ [7].

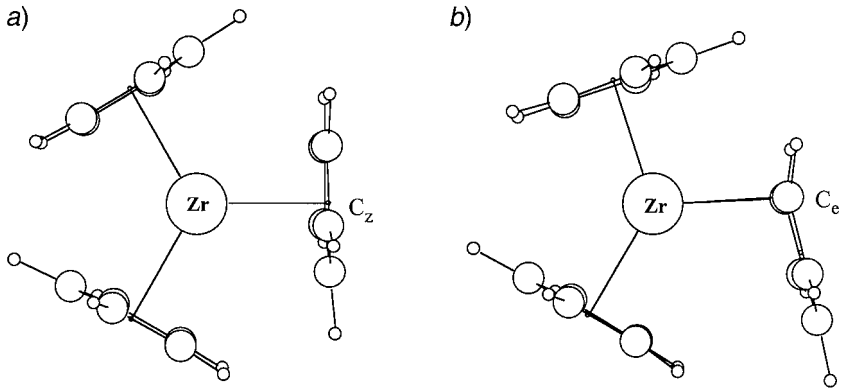


Fig. 2. *Calculated local-minima geometries for* a) $3\eta^5$-$[Zr(Cp)_3]^+$ *and* b) $2\eta^5\eta^2$-$[Zr(Cp)_3]^+$

As a result from this first structural survey of possible geometries for $[Zr(Cp)_3]^+$, we will in the following restrict our discussion to $C_{3h}$-$3\eta^5$ geometries, and the related $2\eta^5\eta^2$ complexes. The assumption that also in the case of Ti and Hf complexes these two coordination modes are the most relevant structures can be justified by analyzing the reasons which rule out the $2\eta^5\eta^1$ and $2\eta^5\eta^3$ modes as coordination geometries. The $2\eta^5\eta^1$ geometry is coordinatively and electronically unsaturated, whereas for the $2\eta^5\eta^3$ case in comparison with the $2\eta^5\eta^2$ geometry, a pair of ligand-based spectator electrons, as we shall see later, is less effectively delocalized. It is not the nature of the transition metal, but rather that of the coordinating ligands which strongly favors $3\eta^5$ and $2\eta^5\eta^2$ complexation.

*[Zr(Cp)$_3$] and [Ti(Cp)$_3$]: Comparison with Experiment.* Two of the molecules under investigation have been structurally characterized by X-ray analysis, namely $[Ti(Cp)_3]$ (**2a**) [9], and $[Zr(Cp)_3]$ (**2b**) [7]. In accord with the experiment, our calculations reveal that $[Zr(Cp)_3]$ prefers $3\eta^5$ coordination, whereas $[Ti(Cp)_3]$ adopts the $2\eta^5\eta^2$ geometry. This fact will be discussed in more detail in the next section. In *Table 1*, we compare a few characteristic geometrical parameters (see also *Fig. 2*). For the $[Zr(Cp)_3]$ molecule with its 3-fold axis, one essential structural parameter is the distance between a ring C-atom and the metal center. The calculated value of 2.60 Å compares well with the experimental value of 2.58 Å. The X-ray structure of $[Ti(Cp)_3]$ shows two different M–$C_z$ distances as well as the $\eta^2$-ligand coordinated in an asymmetric way. In comparison, the optimized M–$C_z$ separations are almost identical, being 0.03 and 0.02 Å longer than those in the crystal. Similarly, the two calculated values of $d$(M–$C_e$) again differ by only 0.01 Å, and are about at the average value of the two experimentally observed distances. Overall, the calculated geometries are in good agreement with those obtained from the X-ray structure analysis.

---

[2]) Geometries based on $C_{3v}$ symmetry have also been considered, they are obtained when the three Cp rings are rotated by 36°. The isomer $C_{3v}$-$3\eta^5$-$[Zr(Cp)_3]^+$ was found to be 24 kJ/mol higher in energy than $C_{3h}$-$3\eta^5$-$[Zr(Cp)_3]^+$.

Table 1. *Comparison of Calculated Geometries with Data from X-Ray Structure Analysis*[a])

| | | $3\eta^5$ | | $2\eta^5\eta^2$ | | |
|---|---|---|---|---|---|---|
| | | M–C[b]) | $\angle C_zMC_z$ | M–$C_e$ | M–$C_z$ | $\angle C_zMC_z$ |
| $[Ti(Cp)_3]$ | exp.[c]) | – | – | 2.42 | 2.04 | 133 |
| | | | | 2.48 | 2.06 | |
| | calc. | – | – | 2.43 | 2.07 | 133 |
| | | | | 2.44 | 2.08 | |
| $[Zr(Cp)_3]$ | exp.[d]) | 2.58 | 120 | – | – | – |
| | calc. | 2.60 | 120 | – | – | – |

[a]) Distances in Å, angles in degree. For the definition of $C_z$ and $C_e$, see *Fig. 2*. [b]) Averaged value. [c]) $2\eta^5\eta^2$-$[Ti(Cp)_3]$ shows the two $\eta^5$-Cp rings in a staggered conformation [9]. [d]) [7].

*$[M(Cp)_3]$ and $[M(Cp)_3]^+$ Systems: $3\eta^5$* vs. *$2\eta^5\eta^2$ Coordination*. Selected geometric data for the optimized geometries for various $[M(Cp)_3]$ systems are collected in *Table 2*. Comparing the related neutral and the cationic compounds, we see that the coordination geometry of the Cp rings bound in an $\eta^5$ fashion is almost identical. Changes, however, are observed for the $\eta^2$-Cp ligand. On going from the neutral to the cationic species, the M–$C_e$ distances, as defined in *Fig. 2*, are becoming significantly shorter. It is interesting to note that the distances $d(M–C_z)$ and $d(M–C_e)$ are increasing in the order Ti < Hf < Zr. Thus, when going from the 4d to the 5d metal, the M–C bond distances decrease, rather than to further increase. This somehow unexpected trend can be explained by relativistic effects. The relativistic core contraction will diminish *Pauli* repulsion and enhance electronic interaction [15]. The consequences are demonstrated in sample calculation on $[Hf(Cp)_3]$ in which the relativistic effects are explicitly excluded. For $3\eta^5$-$[Hf(Cp)_3]$, the value for $d(M–C_z)$ amounts to 2.35 Å, for $2\eta^5\eta^2$-$[Hf(Cp)_3]$, the M–$C_z$ distance now measures 2.60 Å. Non-relativistic calculations indeed result in the monotone trend Ti < Zr < Hf.

Table 2. *Selected Structural Parameters for Various $[M(Cp)_3]$ Systems*[a])

| | $3\eta^5$ | $2\eta^5\eta^2$ | | |
|---|---|---|---|---|
| | M–$C_z$ | M–$C_e$ | M–$C_z$ | $\angle C_zMC_z$ |
| $[Ti(Cp)_3]$ | 2.13 | 2.44 | 2.08 | 133 |
| $[Ti(Cp)_3]^+$ | 2.12 | 2.33 | 2.08 | 133 |
| $[Zr(Cp)_3]$ | 2.31 | 2.53 | 2.27 | 131 |
| $[Zr(Cp)_3]^+$ | 2.30 | 2.45 | 2.26 | 131 |
| $[Hf(Cp)_3]$ | 2.30 | 2.51 | 2.21 | 135 |
| $[Hf(Cp)_3]^+$ | 2.27 | 2.42 | 2.20 | 133 |

[a]) Distances in Å, angles in degree. For the definition of $C_z$ and $C_e$, see *Fig. 2*.

Relative energies of $3\eta^5$ *vs.* $2\eta^5\eta^2$ geometries are presented in *Table 3*. We note that only for the titanium systems, $2\eta^5\eta^2$ is the preferred coordination mode, whereas for the Zr- and Hf-based systems, the $3\eta^5$ mode is at lower energy. However, when going from Zr to Hf, this energy difference decreases; for $[Hf(Cp)_3]^+$ it only amounts to 10 kJ/mol. In all cases, the $2\eta^5\eta^2$ structures are favored on steric grounds, that is in terms of $\Delta E^0$, whereas the $3\eta^5$ geometries are preferred in electronic-interaction energy $\Delta E_{int}$. It is the

Table 3. *Relative Energies* [kJ/mol] *of* $3\eta^5$ *and* $2\eta^5\eta^2$ *Isomers of Various* $[M(Cp)_3]$ *Systems.* The more stable isomer is set to zero.

| | $3\eta^5$ | $2\eta^5\eta^2$ |
|---|---|---|
| $[Ti(Cp)_3]$ | 30 | 0 |
| $[Ti(Cp)_3]^+$ | 38 | 0 |
| $[Zr(Cp)_3]$ | 0 | 36 |
| $[Zr(Cp)_3]^+$ | 0 | 30 |
| $[Hf(Cp)_3]$ | 0 | 20 |
| $[Hf(Cp)_3]^+$ | 0 | 10 |

subtle balance between energy gain in $\Delta E^0$ and energy loss in $\Delta E_{int}$, which only for the titanium case favors $2\eta^5\eta^2$ over $3\eta^5$ coordination.

*Frontier-Orbital Analysis of* $3\eta^5$-$[M(Cp)_3]^+$. The orbital interactions in $[M(Cp)_3]$ systems have already been analyzed [2][3], and we shall briefly summarize these results. The original analysis of *Lauher* and *Hoffmann* was based on the $[Ti(Cp)_3]$ fragment with $C_{3v}$ symmetry. The three $Cp^-$ ligands can potentially donate 18 electrons to the Ti-center. One of the resulting donor orbitals, however, is of $a_2$ symmetry and has no metal-based counterpart. This is a special case of the three-fold symmetry, and can also be found in other systems having a $C_3$ axis, like $[W(RC{\equiv}CR)_3(CO)]$ [16a]. Thus, the $(Cp)_3^-$ fragment has to be considered only as a 16-$e^-$ donor. This results in one ligand-based spectator electron pair, and one orbital on the metal fragment, available for chemical bonding. For the $[M(Cp)_3]^+$ systems under investigation, this metal-based $d_{z^2}$ orbital is empty and represents the LUMO. In $C_{3h}$ symmetry, the relevant orbital of the $(Cp)_3^-$ fragment now transforms according to a′ symmetry, and could in principle interact with the metal center. However, a proper spatial match of the two sets of orbitals is still not possible, which again is caused by the three-fold symmetry axis. A population analysis reveals that the principal orbital characteristics are the same in $C_{3v}$ as well as in $C_{3h}$ symmetry; the HOMO of $[M(Cp)_3]^+$ is solely based on the Cp ligands, and the LUMO corresponds to a $d_{z^2}$ orbital. These two important orbitals are depicted in *Fig. 3*.

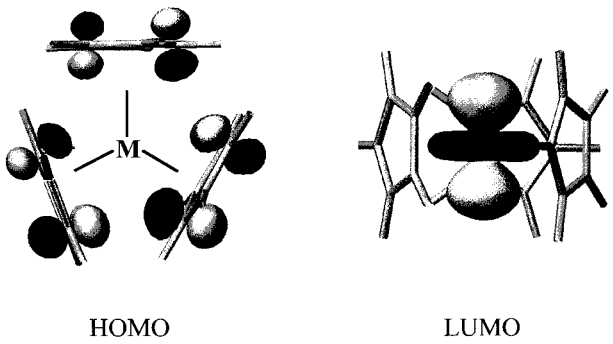


Fig. 3. *HOMO and LUMO of* $[M(Cp)_3]^+$, *the former being based on the Cp ligands and the latter being a metal-based* $d_{z^2}$ *orbital*

It is also noteworthy that the main orbital characteristics, one empty metal-based orbital and one ligand-based electron pair, are also conserved under ring slippage from $3\eta^5$ to $2\eta^5\eta^2$. Also, the composition of the HOMO stays essentially the same, so that a second-order *Jahn-Teller* distortion [16b] can be excluded as driving force for the geometry distortion.

*Complexes of [M(Cp)$_3$]$^+$ with Donor Ligands.* We now consider the interaction of the $[M(Cp)_3]^+$ fragments with the ligands carbon monoxide, methyl isonitrile, and acetonitrile. The geometry optimization revealed that in all cases, the coordination of the $M(Cp)_3$ moiety in $[M(Cp)_3(L)]^+$ resembles that of the free $[M(Cp)_3]^+$. In particular, the Zr and Hf systems show a $3\eta^5$-type coordination, whereas Ti again prefers a $2\eta^5\eta^2$ arrangement. An exemplary structure for $[Zr(Cp)_3(N{\equiv}CMe)]^+$ (**3d**) is shown in *Fig. 4*, and representative geometric parameters are collected in *Table 4*. We want to point out that all ligands including the isonitrile stay linear under coordination, and do not bend.

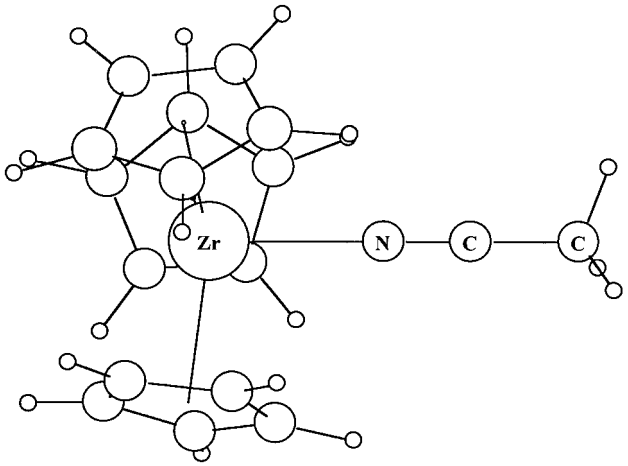


Fig. 4. *Optimized DFT geometry of [Zr(Cp)$_3$(N≡CMe)]$^+$* (**3d**)

Table 4. *Selected Structural Parameters*[a]) *for [M(Cp)$_3$(L)]$^+$ Complexes* (M = Ti, Zr, Hf; L = CO, C≡NMe, N≡CMe)

| | M–C$_z$[b]) (M–C$_e$)[c]) | ∠C$_z$MC$_z$[b]) | M–L | C–O/C–N[d]) |
|---|---|---|---|---|
| $[Ti(Cp)_3(CO)]^+$ | 2.07 (2.40, 2.44) | 132 | 2.09 | 1.15 |
| $[Ti(Cp)_3(C{\equiv}NMe)]^+$ | 2.09 (2.38, 2.47) | 132 | 2.15 | 1.17 |
| $[Ti(Cp)_3(N{\equiv}CMe)]^+$ | 2.09 (2.35, 2.50) | 139 | 2.18 | 1.16 |
| $[Zr(Cp)_3(CO)]^+$ (**3c**) | 2.35 | 119 | 2.25 | 1.14 |
| $[Zr(Cp)_3(C{\equiv}NMe)]^+$ (**3e**) | 2.34 | 119 | 2.30 | 1.17 |
| $[Zr(Cp)_3(N{\equiv}CMe)]^+$ (**3d**) | 2.32 | 119 | 2.32 | 1.16 |
| $[Hf(Cp)_3(CO)]^+$ (**9b**) | 2.33 | 119 | 2.22 | 1.15 |
| $[Hf(Cp)_3(C{\equiv}NMe)]^+$ (**9a**) | 2.33 | 119 | 2.25 | 1.17 |
| $[Hf(Cp)_3(N{\equiv}CMe)]^+$ | 2.31 | 118 | 2.28 | 1.16 |

[a]) Distances in Å, angles in degree. [b]) C$_z$ is the center of an $\eta^5$-bonded Cp ring (see *Fig. 2*). [c]) The data in parentheses refer to an $\eta^2$-bonded Cp ring. C$_e$ denotes a ring C-atom bonded to the metal (see *Fig. 2*). [d]) Optimized distances $d$(C–O) and $d$(C–N) for the free ligands are: CO, 1.14 Å; C≡NMe, 1.18 Å; N≡CMe; 1.16 Å.

When comparing the fragment geometries in the donor complexes to that of the donor-free complex, one finds that the distances of the centroids of the $\eta^5$-bonded Cp rings to the metal center increases by *ca.* 0.03 Å. However, for the $3\eta^5$ structures, the angle $C_z$–M–$C_z$ is still close to 120°. In this case, the metal centers are not in a tetrahedral coordination. The LUMO, which is exclusively a metal based $d_{z^2}$ is apparently not involved in any hybridization. Interesting is the case for the $2\eta^5\eta^2$-bonded titanium systems. Here, we find that the $\eta^2$-bonded Cp ring adopts an asymmetric coordination, with one short and one longer M–$C_e$ distance. The Cp ligand has the tendency to change its coordination mode from $\eta^2$ to $\eta^1$ under coordination of the donor ligand[3]). The general trend in the M–L bond lengths is Ti < Hf < Zr, caused by relativistic effects, as discussed above. For the ligands, we observe the following ranking in the metal-to-ligand distance: CO < CNMe < NCMe. For the nitrile and isonitrile ligands, the calculated M–L separation is in close agreement with the experiment, whereas for the case of CO, the calculated M–CO distance falls short by 0.06 Å.

The change of the C–N or the C–O distances of the ligands under coordination to the metal center might give some indication about the nature of this bond. We find as a general trend that the C–O distance increases by 0.01 Å, the C–NMe distances shortens by the same amount, and the N–CMe distance roughly stays the same. One argument for a C–O or C–N bond shortening under coordination to the metal center is that of increased $\sigma$ donation. The $5\sigma$ orbital in CO is assumed to possess some C–O antibonding character [16c]. Hence, OC → M donation should remove electron density from this orbital, and consequently strengthen and shorten the bond. The same holds for the other two ligands. Although the systems under investigation all possess a $d^0$ metal center, back bonding is still possible through filled Cp–Zr functions, mainly based on the Cp ligands. If one takes the *Mulliken* population on all virtual $[M(Cp)_3]$ orbitals and on all virtual L orbitals as a measure for $\sigma$ donation and $\pi$ backdonation, one finds average $\sigma/\pi$ ratios of 1.0, 1.5, and 2.9 for CO, CNMe and NCMe, respectively. According to this, one would expect the most pronounced bond shortening to occur in the case of acetonitrile, in contrast to the results obtained here. However, *Goldman* and *Krogh-Jespersen* have recently shown how electrostatic effects are responsible for C–O bond shortening [17]. We will analyze this aspect in more detail in the next section.

*Bond Analysis for M–L in $[M(Cp)_3(L)]^+$ Complexes.* We analyze the M–L bond in $[M(Cp)_3(L)]^+$ according to the scheme outlined in *Eqn. 1*. The results of this procedure are collected in *Table 5* and *Fig. 5*. As a general trend, one finds an increasing bond strength when going down the triad. Further, it can be seen that CO forms the weakest bonds to the metal center, and the isonitrile the strongest. To rationalize this, we will evaluate the terms for *Pauli* repulsion and orbital interaction together as the orbital energy $\Delta E_{orb}$ (*Eqn. 3*). Accordingly, the bonding energy now is broken up into one orbital term and one electrostatic term (*Eqn. 4*).

$$\Delta E_{orb} = \Delta E_{Pauli} + \Delta E_{int} \tag{3}$$

$$BE = -[\Delta E_{orb} + \Delta E_{elstat}] \tag{4}$$

---

[3]) The same was found for $[Ti(Cp)_3(Me)]$: the $C_2$–Ti distances amount to 2.39 and 2.63 Å. A $2\eta^5\eta^1$ geometry ($d$(Ti–$C_e$) = 2.33 and 2.88 Å) is more stable by 4 kJ/mol, whereas the $3\eta^5$ structure is 39 kJ/mol higher in energy.

The orbital terms $\Delta E_{orb}$ are destabilizing, since in all cases the *Pauli*-repulsion term outweighs the electronic interaction (*cf. Table 5*). It is evident that in terms of the orbital energy, the ligands CO and CNMe are comparable, but also that the latter undergoes an enhanced electrostatic interaction with the metal fragment. This electrostatic interaction, together with a reduced $\sigma/\pi$ ratio leads to a C–N bond shortening under complexation. Acetonitrile shows a reduced electrostatic interaction, but also the least destabilizing orbital terms (mainly caused by a significant decrease in *Pauli* repulsion; *cf. Table 5*), leading to bonds of moderate strength.

Table 5. *Energy Decomposition* [kJ/mol] *for the M–L Bond in* $[M(Cp)_3(L)]^+$ *Complexes* (M = Ti, Zr, Hf; L = CO, C≡NMe, N≡CMe)

| | $\Delta E_{elstat}$ | $\Delta E_{Pauli}$ | $\Delta E_{int}$ | *BE* |
|---|---|---|---|---|
| OC–Ti | – 282 | 476 | – 302 | 108 |
| MeNC–Ti | – 337 | 414 | – 246 | 169 |
| MeCN–Ti | – 233 | 261 | – 164 | 136 |
| OC–Zr | – 228 | 365 | – 247 | 110 |
| MeNC–Zr | – 309 | 345 | – 218 | 182 |
| MeCN – Zr | – 219 | 223 | – 155 | 151 |
| OC–Hf | – 288 | 448 | – 294 | 134 |
| MeNC–Hf | – 390 | 457 | – 274 | 207 |
| MeCN–Hf | – 264 | 186 | – 192 | 170 |

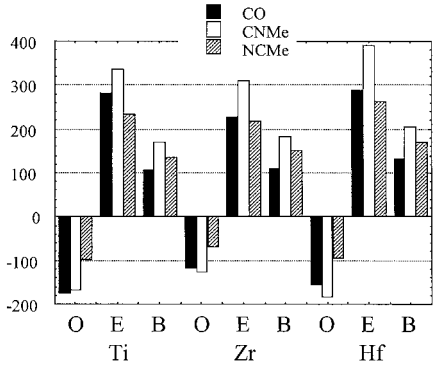


Fig. 5. *Energy decomposition for the M–L bond in* $[M(Cp)_3(L)]^+$ *complexes according to orbital terms and electrostatic terms.* The negative of $\Delta E_{orb}$ (O) and $\Delta E_{elsat}$ (E) is shown, so that in any case, positive energy values indicate stabilization; B stands for the bonding energy *BE*.

*Conclusion of the Theoretical Study.* The $[M(Cp)_3]^+$ systems are likely to be isostructural to their neutral counterparts $[M(Cp)_3]$, showing $3\eta^5$-coordination geometries for Zr and Hf, and a $2\eta^5\eta^2$ geometry for Ti. All the $[M(Cp)_3]^+$ have to be considered as 16-e$^-$ complexes, with one empty metal-based d orbital available for bonding. Under coordination of a donor ligand, the geometry of the $[M(Cp)_3]$ fragment is preserved for Zr and Hf, whereas for Ti, the $\eta^2$-bonded Cp ring changes its coordination mode towards an $\eta^1$ mode. This and the fact that Ti forms the weakest bond to donor ligands suggests that the $[Ti(Cp)_3(L)]^+$ species should be not so stable as

its heavy-metal counterparts. Isonitrile ligands form strong metal-ligand bonds, due to an enhanced electrostatic interaction.

2.2. *Experimental Studies.* The cationic tris(cyclopentadienyl)(group-4 metal) complexes were prepared according to the synthetic scheme that we had successfully applied for the synthesis of the $[Zr(Cp)_3]^+$ complexes **3** [10]. For this purpose, the respective metallocene(2+) dichlorides **4** were converted to their $\mu$-oxo-bis-metallocene chlorides **5** by stoichiometric treatment with water in the presence of aniline [18] (*Scheme 1*). Subsequent reaction with trimethylaluminum gave the $[MCl(Cp)_2(Me)]$ complexes **6** [19] that were then treated with sodium cyclopentadienide to yield the $[M(Cp)_3(Me)]$ complexes **7a** (M=Ti), **7b** (M=Zr) [10], and **7c** (M=Hf), respectively. For **7c**, a fully satisfying elemental analysis could not be obtained; however, comparison of its spectroscopic properties with that of **7b** established that these complexes are isostructural.

In a few preliminary experiments, several methyl-anion abstractions starting from $[Hf(Cp)_3(Me)]$ (**7c**) were tested in NMR experiments using deuterated solvents. Treatment of **7c** with either trityltetraphenylborate [20] or *N,N*-dimethylanilinium tetraphenylborate [21] in $CD_2Cl_2/(D_8)THF$ 10:1 generated $[Hf(Cp)_3(THF)]^+$[4] (**8**·THF[4]); with counterion $[BPh_4]^-$; $^1$H-NMR: $\delta$ 6.30 (Cp)) (see *Scheme 2*). Analogously, treatment of **7c** with the organometallic *Lewis* acid tris(pentafluorophenyl)borane [22] led to the generation of $[Hf(Cp)_3]^+[B(C_6F_5)_3(Me)]^-$ (**8**·$[B(C_6F_5)_3(Me)]^-$). The cation formation is established by a strong shift of the $^1$H-NMR resonance ($CD_2Cl_2$) to higher $\delta$ values as compared to the neutral starting material **7c** (**7c** (room temp.): $\delta$ 5.69

*Scheme 1*

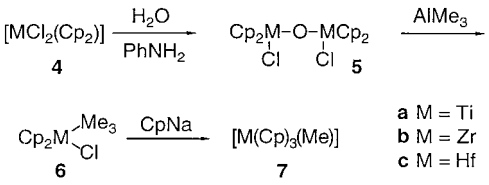


*Scheme 2*

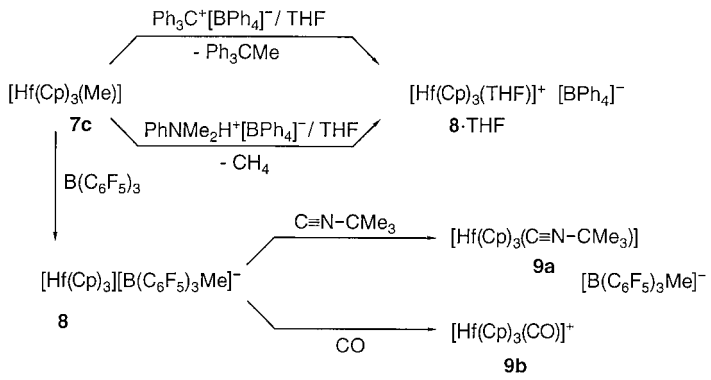


[4]) For convenience, THF is used in formulae also when $(D_8)$THF is meant.

(*s*, 3 Cp), and 0.20 (*s*, Me); **8e**·[$B(C_6F_5)_3(Me)]^-$ (243 K): $\delta$ 6.21 (*s*, 3 Cp) and 0.42 (br. *s*, MeB)).

We used the $Me^-$ abstraction reaction with $B(C_6F_5)_3$ [22b] to prepare the ligand-stabilized complex $[Hf(Cp)_3(C{\equiv}N{-}CMe_3)]^+$ (**9a**; isolated with counterion $[B(C_6F_5)_3(Me)]^-$ (*Scheme 2*). A procedure was applied that involved the *in situ* generation of the reactive $[Hf(Cp)_3]^+$ cation (**8**) from **7c** in the non-coordinating solvent $CH_2Cl_2$ at low temperature, which was then instantaneously trapped by *tert*-butyl isocyanide, present in the solution, to form the stable complex **9a**·$[B(C_6F_5)_3(Me)]^-$ as a yellow crystalline material in 45% yield (see *Exper. Part*). Complex **9a**·$[B(C_6F_6)(Me)]$ is characterized by its $^1$H-NMR ($CD_2Cl_2$, 243 K) data $\delta$ 5.81 (*s*, 3 Cp), 1.72 (*s*, *t*-Bu), and 0.42 (br. *s*, Me–B) and its IR $\tilde{\nu}$(C≡NR), band at 2211 $cm^{-1}$ ($\tilde{\nu}$ 2140 $cm^{-1}$ for free *tert*-butyl isocyanide). Complex cation **9a** behaved as a typical charged $d^0$-configurated isocyanide(transition metal) complex [23] where the electrostatic component of the metal-isonitrile linkage probably dominates the spectroscopic and structural appearance [17] (see below) of the Hf ← C≡N–R moiety. Spectroscopically, complex cation **9a** behaves quite analogously to the corresponding complex cation $[Zr(Cp)_3(C{\equiv}N{-}CMe_3)]^+$ (**3e**; IR: $\tilde{\nu}$(C≡NR) 2209 $cm^{-1}$) that we have previously described [10a].

Treatment of the system $[Hf(Cp)_3]^+[B(C_6F_5)_3(Me)]^-$ (**8**·$[B(C_6F_5)_3(Me)]^-$), *in situ* generated from $[Hf(Cp)_3(Me)]$ (**7c**) and $B(C_6F_5)_3$, with carbon monoxide in $CH_2Cl_2$ solution at 0° gave the corresponding cationic carbonyl($d^0$-metal) complex $[Hf(Cp)_3(CO)]^+$ (**9b**; with counterion $[B(C_6F_5)_3(Me)]^-$). Crystalline **9b**·$[B(C_6F_5)_3(Me)]^-$ was obtained from $CH_2Cl_2$ at −30°. Complex cation **9b** shows typical $^1$H- and $^{13}$C-NMR signals (Cp *s* at $\delta$(H) 5.94 and $\delta$(C) 110.4, and $\delta$(C) of CO at $\delta$ 201.0) which are very similar to those of the related zirconium complex cation $[Zr(Cp)_3(CO)]^+$ (**3c**; with counterion $[B(C_6F_5)_3(Me)]^-$ [10a]) (Cp at $\delta$(H) 6.05 and $\delta$(C) 112.7, $\delta$(C) of CO at 206.9). The IR $\tilde{\nu}$(CO) of **9b** at 2137 $cm^{-1}$ is at an only marginally lower wavenumber than found for **3c** (2150 $cm^{-1}$) and free CO (2143 $cm^{-1}$). A satisfactory elemental analysis of **9b**·$[B(C_6F_5)_3(Me)]^-$ could not be obtained.

Single crystals were obtained of both complexes **9a**·$[B(C_6F_5)_3(Me)]$ and **9b**·$[B(C_6F_5)_3(Me)]$ that allowed a characterization by X-ray crystal-structure analyses. The cation carbonyltris(cyclopentadienyl)hafnium(1+) (**9b**) is clearly separated from its $[B(C_6F_5)_3(Me)]^-$ anion in the crystal. The $Hf(Cp)_3$ moiety in $[Hf(Cp)_3(CO)]^+$ is of the $3\eta^5$-structural type [24]. The Hf–C(Cp) bond lengths of the three individual Cp ligands are as follows (for atom numbering see *Fig. 6*): Hf–C(11) to C(15): 2.587(14), 2.539(12), 2.526(16), 2.550(17), 2.618(14) Å; Hf–C(21) to C(25): 2.527(13), 2.589(10), 2.570(14), 2.544(12), 2.478(15) Å; Hf–C(31) to C(35): 2.545(14), 2.599(15), 2.611(13), 2.507(13), 2.541(14) Å. This amounts to an average Hf–C(Cp) bond length of *ca.* 2.55 ± 0.07 Å. The uniform and narrow range of these Hf–C separations clearly indicates the presence of three uniformly $\eta^5$-coordinated Cp ligands that are bonded to the central transition-metal center in an almost symmetry-equivalent manner. The three Cp ligands are arranged at the Hf-atom in such a way that their centroids can be regarded to form the basal plane of a trigonal-pyramidal coordination polyhedron around Hf. The average D–Hf–D angle (D denotes the centroids of the respective Cp ligands) in the cation **9b** is 119.3° (individual values: D(1)–Hf–D(2) 118.6°; D(1)–Hf–D(3) 120.1°; D(2)–Hf–D(3) 119.1°), which is very

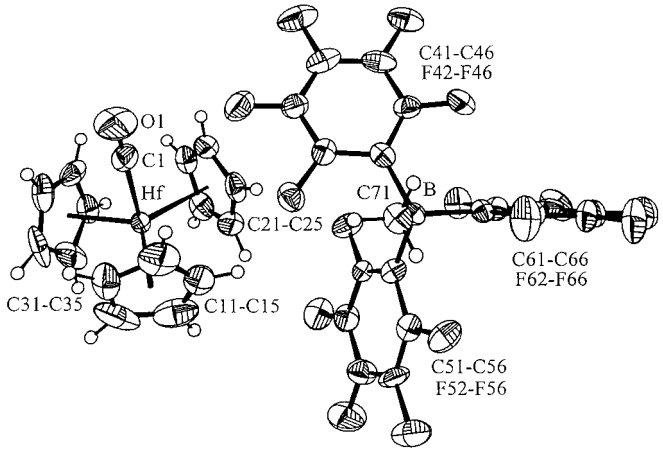


Fig. 6. *A view of the molecular structure of the salt* $[Hf(Cp)_3(CO)]^+[B(C_6F_5)_3(Me)]^-$ (**9b** · $[B(C_6F_5)_3(Me)]^-$). Selected bond lengths [Å] and angles [°]: Hf–C(1) 2.271(12), C(1)–O(1) 1.108(15), Hf–C(Cp) 2.55, B–C(41) 1.67(2), B–C(51) 1.65(2), B–C(61) 1.66(2), B–C(71) 1.64(2); Hf–C(1)–O(1) 178.4(13), C(41)–B–C(51) 114.1(9), C(41)–B–C(61) 110.9(9), C(41)–B–C(71) 103.1(9), C(51)–B–C(61) 103.6(9), C(51)–B–C(71) 110.7(9), C(61)–B–C(71)114.8(10).

close to the expected 120° angle of this idealized bonding situation. Accordingly, the D–Hf–C(1) angles average to a value of 95.0° (individual values: C(1)–Hf–D(1) 94.3°; C(1)–Hf–D(2) 96.5°; C(1)–Hf–D(3) 94.1°), which is not too far from the ideal 90° angle of the trigonal pyramid. Consequently, the Hf-atom is located only 0.196 Å above the plane determined by the centroids of the three $\eta^5$-Cp ligands. In this arrangement, the CO ligand is placed at the apex of the trigonal pyramid. The Hf–C(1) bond length is 2.271(12) Å, and the C(1)–O(1) bond is very short at 1.108(15) Å, which is almost identical with free CO. The Hf–C(1)–O(1) unit is linear (178.4(13)°). A comparison with the very similar values of the cation $[Zr(Cp)_3(CO)]^+$ (**3c**) is given in *Table 6*.

The structure of the cation $[Hf(Cp)_3(C{\equiv}N{-}CMe_3)]^+$ (**9a**) in the crystal (*Fig. 7*) is very similar to that of **9b**. Again, the three Cp ligands are $\eta^5$-coordinated to the Hf-center (average Hf–C(Cp) bond length: 2.566 Å). The complex **9a**, therefore, also

Table 6. *A Comparison of Characteristic Structural Parameters of* $[M(Cp)_3(L)]^+$ *Complexes* **9** (M=Hf) *and* **3** (M=Zr). D denotes the centroid of the three Cp ligands.

| | **9a** | **3e**[a]) | **9b** | **3c**[a]) |
|---|---|---|---|---|
| M | Hf | Zr | Hf | Zr |
| L | $CNCMe_3$ | $CNCMe_3$ | CO | CO |
| M–C(1) [Å] | 2.275(4) | 2.313(3) | 2.271(12) | 2.311(6) |
| C(1)–N(O) [Å] | 1.146(5) | 1.145(4) | 1.108(15) | 1.110(7) |
| D–M–D [°][b]) | 118.8 | 118.7 | 119.3 | 119.0 |
| C(1)–M–D [°][b]) | 96.5 | 96.6 | 95.0 | 95.7 |
| M···$D_3$ [Å][c]) | 0.257 | 0.229 | 0.196 | 0.229 |
| M–C(Cp) [Å][b]) | 2.566 | 2.580 | 2.55 | 2.583 |

[a]) From [10a]. [b]) Averaged value. [c]) Distance of the metal center to the basal $D_3$ plane.

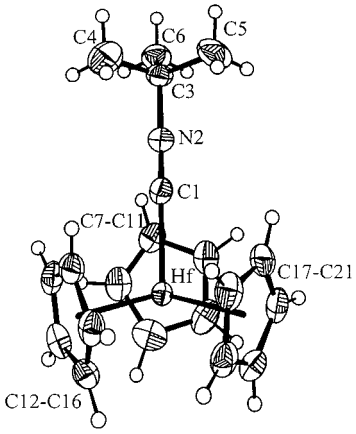


Fig. 7. *Molecular geometry of* **9a** (cation only). Selected bond lengths [Å] and angles [°] ($[B(C_6F_5)_3(Me)]^-$ anion) Hf–C(1) 2.275(4), C(1)–N(2) 1.146(5), N(2)–C(3) 1.471(5), Hf–C(7) 2.540(4), Hf–C(8) 2.639(4), Hf–C(9) 2.607(4), Hf–C(10) 2.540(3), Hf–C(11) 2.530(3), Hf–C(12) 2.534(3), Hf–C(13) 2.522(3), Hf–C(14) 2.610(3), Hf–C(15) 2.588(3), Hf–C(16) 2.542(3), Hf–C(17) 2.593(3), Hf–C(18) 2.615(3), Hf–C(19) 2.544(3), Hf–C(20) 2.540(4), Hf–C(21) 2.547(4), Hf–C(Cp) 2.566, B–C(22) 1.647(5), B–C(30) 1.652(5), B–C(40) 1.654(5), B–C(50) 1.664(5); Hf–C(1)–N(2) 178.8(3), C(1)–N(2)–C(3) 179.0(4), D(1)–Hf–D(2) 118.7, D(1)–Hf–D(3) 118.9, D(2)–Hf–D(3) 118.7, C(1)–Hf–D(1) 95.7, C(1)–Hf–D(2) 96.9, C(1)–Hf–D(3) 96.9, C(22)–B–C(30) 112.0(3), C(22)–B–C(40) 107.9(3), C(22)–B–C(50) 106.5(3), C(30)–B–C(40) 107.5(3), C(30)–B–C(50) 110.6(3), C(40)–B–C(50) 112.3(3).

belongs to the $3\eta^5$-structural type (see *Fig. 1*). The average D–Hf–D angle of **9a** is 118.8°, and the Hf-atom is located 0.257 Å above the $D_3$-basal plane of the trigonal-pyramidal coordination polyhedron (*Table 6*). The Hf–C(1) bond is 2.275(4) Å. The C(1)–N(2) bond length in the isonitrile ligand amounts to 1.146(5) Å (free uncoordinated isonitrile: 1.145 Å [25]). The Hf–C(1)–N(2)–C(3) unit is linear (angles Hf–C(1)–N(2) 178.8(3)°, C(1)–N(2)–C(3) 179.0(4)°). The overall conformational arrangement of **9a** is eclipsed (as in the related cation $[Zr(Cp)_3(C{\equiv}N{-}CMe_3)]^+$ (**3e**) [10a], see above).

The experimental studies with the corresponding $Ti(Cp)_3$-derived systems have turned out to be more difficult so far. Therefore, we must rely more on the results of the theoretical calculations (see above) in this area for the structure characterization of these tris(cyclopentadienyl)metal complexes. The neutral complex $[Ti(Cp)_3(Me)]$ (**7a**) was prepared according to *Scheme 1* and isolated in 65% yield. Complex **7a** shows a $^1$H-NMR *s* at $\delta$ 0.21 (3H) for the Me–Ti group in ($D_8$) toluene at 313 K and a broad Cp *s* (15H) at $\delta$ 5.50. Lowering the monitoring temperature rapidly leads to substantial broadening of the latter signal and eventually splitting into two *s* at $\delta$ 5.95 and 5.20 in a 5:10 ratio, whereas the Me resonance remains unaffected. In $CD_2Cl_2$, a similar behavior is observed, except that in this case, the order of the $^1$H-NMR Cp-signals is reversed. At low temperature (183 K), the low-field *s* ($\delta$ 5.83) corresponds to two symmetry-equivalent Cp ligands, whereas the *s* at $\delta$ 5.30 represents a single Cp-ligand at the Ti-center (Me *s* again observed at $\delta$ 0.22 ppm under these conditions). This observation reveals a 2:1 differentiation of the Cp ligands in complex $[Ti(Cp)_3(Me)]$ (**7a**), in contrast to $[Zr(Cp)_3(Me)]$ (**7b**) and $[Hf(Cp)_3(Me)]$ (**7c**). In view of the

observations previously made for $[Ti(Cp)_4]$, it is very likely that the titanium complex **7a** contains two $\eta^5$-coordinated Cp ligands and a $\sigma$-bound Cp group (*i.e.* $\eta^1$-Cp), only that the latter even at 183 K in $CD_2Cl_2$ still undergoes a rapid metallotropic (*i.e.* 1,5-sigmatropic) shift of the $Cp_2(Me)Ti$-substituent at the $\sigma$-cyclopentadienyl ligand [26]. Of course, alternative formulations involving, *e.g.*, a $\eta^2$-Cp situation cannot be ruled out as long as the low-barrier dynamic process that leads to the internal equilibration of the third, low-hapticity Cp ligand is not frozen out. We have tried to achieve this experimentally in solution by using $CDFCl_2$ as a solvent for the low-temperature $^1$H-NMR measurement of **7a**, but only a substantial reversible broadening of the Cp resonances was achieved at the lowest temperature of 138 K (with the Me resonance still remaining sharp), but freezing of the remaining dynamic process on the 600-MHz $^1$H-NMR time scale and resolution of the low-hapticity Cp-ligand signals under static conditions could not be achieved up to now.

Tris(cyclopentadienyl)titanium cation **10** was generated by treatment of $[Ti(Cp)_3(Me)]$ (**7a**) with $B(C_6F_5)_3$ in $CD_2Cl_2$ (*Scheme 3*). We tried to use the *in situ* generated species **10** as a starting material for the formation of ligand-stabilized $[Ti(Cp)_3(L)]^+$ species, but reactions with $C{\equiv}NCMe_3$ or CO have failed so far to produce adducts sufficiently clean for a characterization. It is unclear at present whether such complexes are unstable under the applied reaction conditions or if the reactions with carbon monoxide or isonitriles lead to more complicated reaction schemes (*e.g.* involving insertion reactions in addition to simple adduct formation) in the case of the titanium complexes.

*Scheme 3*

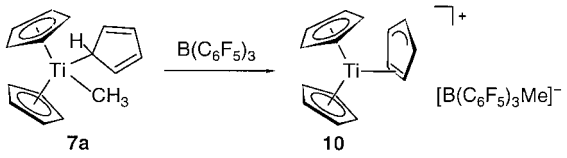


The in the solvent $CDFCl_2$ *in situ* generated system $[Ti(Cp)_3]^+[B(C_6F_5)_3(Me)]^-$ (**10**·$[B(C_6F_6)_3(Me)]^-$) shows a broad $^1$H-NMR Me resonance of the anion in addition to a single Cp resonance (15H) at $\delta$ 6.96 at 213 K (600 MHz). The Cp signal rapidly gets broad upon lowering the temperature and splits into five well-resolved signals in a 2 : 5 : 2 : 5 : 1 ratio at 143 K. This clearly indicates that one Cp ring in $[Ti(Cp)_3]^+$ is bonded in a lower-hapticity mode than $\eta^5$ coordination. In view of the theoretical results (see above), it is likely that the $[Ti(Cp)_3]^+$ cation exhibits a $2\eta^5\eta^2$-type structure and thus contains two diastereotopic $\eta^5$-Cp ligands ($^1$H-NMR signals at $\delta$ 7.06 and 6.70 (each 5H)) and a $\eta^2$-cyclopentadienyl ligand that is arranged at the bent metallocene wedge in such a way that it is bisected by the 'vertical' bent metallocene mirror plane, making the atoms C(1)/C(2) and C(3)/C(4) pairwise symmetry equivalent (see *Scheme 3*). Consequently, a set of three $^1$H-NMR signals is observed at 143 K for the Ti-bound $\eta^2$-Cp ligand, at $\delta$ 7.80 (2H), 6.89 (2H), and 6.34 (1H) (see *Fig. 8*).

This combined experimental and theoretical study thus revealed that there are major structural differences between $[Ti(Cp)_3]^+$ and the pair of its heavier analogues $[Zr(Cp)_3]^+$ and $[Hf(Cp)_3]^+$. The first-row group-4 metal complex exhibits a tendency

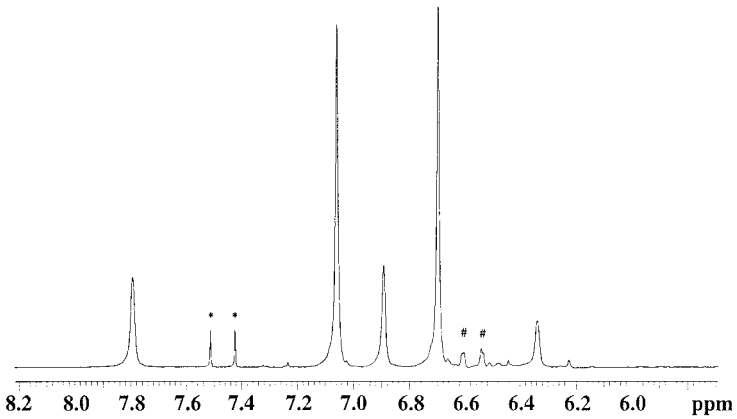


Fig. 8. *$^1$H-NMR Spectrum* (600 MHz) *of [Ti(Cp)$_3$]$^+$[B(C$_6$F$_5$)$_3$(Me)]$^-$* (**10**) (cation signals only) *in CDFCl$_2$ at 143 K, indicating the presence of a 2$\eta^5\eta^2$-type structure.* *, residual CHFCl$_2$ solvent; #, impurity.

of having one of its Cp ligands bonded in a lower hapticity mode than $\eta^5$-coordination. Both the Zr and the Hf systems appear to favor high-symmetry 3$\eta^5$-type structures unless steric factors overcome this electronic control and start to dominate the overall structural picture. In view of the smaller covalent radii and slightly thermodynamically stronger $\sigma$-bonds, this influence is more likely to set in in the case of Hf than Zr.

Financial support from the *Fonds der Chemischen Industrie*, the *Ministerium für Wissenschaft und Forschung des Landes NRW* (*G. E.*), and from the *Swiss National Science Foundation* (*H. B.*), as well as access to the computing facilities of the Rechenzentrum der Universität Zürich is gratefully acknowledged.

## Experimental Part

1. *General*. All reactions were carried out under Ar using *Schlenk*-type glassware or in a glove-box. Solvents, including deuterated solvents used for NMR spectroscopy, were dried and distilled under At prior to use. Tris(pentafluorophenyl)borane [22a], [HfCl(Cp)$_2$(Me)], and [TiCl(Cp)$_2$(Me)] were prepared according to [18][19]. M.p.: *DSC 2010* (*Texas Instruments*). IR Spectra: *Nicolet-5-DXC-FT* IR spectrometer; in cm$^{-1}$. NMR Spectra: *Bruker-AC-200P* ($^1$H 200 MHz, $^{13}$C 50 MHz) and *Varian-Unity-Plus* ($^1$H 599.9 MHz, $^{13}$C 150.9 MHz) spectrometer; $\delta$ in ppm, *J* in Hz. Elemental analyses: *Foss Heraeus CHNO Rapid*.

2. *Syntheses and NMR Studies. Tris($\eta^5$-cyclopentadienyl)methylhafnium* (**7c**). A soln. of [HfCl(Cp)$_2$(Me)] (**6c**; 2.30 g, 6.40 mmol) in toluene (50 ml) was added dropwise to a suspension of sodium cyclopentadienide (0.75 g, 8.53 mmol) in toluene (30 ml). The turbid mixture turned yellow and was stirred overnight at r.t. The solid was removed by filtration and the filtrate evaporated. The residue was suspended in pentane (30 ml) and the solid precipitate collected by filtration: 1.92 g (77%) of **7c**. M.p. 194°. IR (KBr): 3089, 2917, 2874, 2830, 1440, 1145, 846. $^1$H-NMR ((D$_6$)benzene): 5.38 (*s*, 3 Cp); 0.36 (*s*, Me). $^1$H-NMR ($CD_2Cl_2$): 5.69 (*s*, 3 Cp); 0.20 (*s*, Me). $^{13}$C-NMR ((D$_6$)benzene): 110.5 (Cp); 20.1 (Me). Anal. calc. for $C_{16}H_{18}Hf$ (388.8): C 49.43, H 4.76; found: C 48.43, H 4.67.

*Generation of Tris($\eta^5$-cyclopentadienyl)hafnium(1+) Methyltris(pentafluorophenyl)borate(1−)* (**8**·[B(C$_6$F$_5$)$_3$(Me)]$^-$) *in $CD_2Cl_2$ Solution.* A soln. containing **7c** (10.0 mg, 25.7 µmol) in $CD_2Cl_2$ (*ca.* 300 µl) was combined with a B(C$_6$H$_5$)$_3$ soln. (16.9 ml, 33.4 µmol) in the same volume of $CD_2Cl_2$. The product soln. was directly monitored by NMR spectroscopy. $^1$H-NMR ($CD_2Cl_2$, 243 K): 6.21 (*s*, 3 Cp); 0.42 (*s*, Me–B). $^{13}$C-NMR ($CD_2Cl_2$, 243 K): 115.0 (Cp); Me–B not observed.

*Tris($\eta^5$-cyclopentadienyl)[2-(isocyano-$\kappa$N)-2-methylpropane]hafnium(1+) Methyltris(pentafluorophenyl)-borate(1−)* (**9a**·[B(C$_6$F$_5$)(Me)]$^-$). A *Schlenk* flask was charged with a mixture of the solids **7c** (100 mg, 257 µmol) and B(C$_6$F$_5$)$_3$ (171 mg, 334 µmol). Then a cold (− 78°) soln. containing 2-isocyano-2-methylpropane (0.15 ml, 107 mg, 1.29 mmol) in $CH_2Cl_2$ (10 ml) was slowly added. The mixture was stirred for 1 h at − 78° and

then slowly warmed to r.t. The mixture was concentrated *in vacuo* to *ca.* 1/2 volume and the product precipitated by the addition of pentane and collected by filtration: 114 mg (45%). Single crystals of **9a**·[$B(C_6F_5)_3(Me)]^-$ suited for the X-ray crystal-structure analysis were obtained from $CH_2Cl_2$ at $-30°$. M.p. 116°. IR (KBr): 3138, 2990, 2952, 2917, 2211, 1641, 1511, 1457, 1266, 1081, 957, 816. $^1$H-NMR ($CD_2Cl_2$, 600 MHz, 243 K): 5.81 (*s*, 3 Cp); 1.72 (*s*, *t*-Bu); 0.42 (br. *s*, Me–B). $^{13}$C-NMR ($CD_2Cl_2$, 150.9 MHz, 243 K): 147.3 ($^1J$(C,F) = 233), 136.7 ($^1J$(C,F) = 243), 135.6 ($^1J$(C,F) = 222, $C_o$, $C_p$, $C_m$ ($C_6F_5$)); 127.7 (br. *s*, $C_{ipso}$ ($C_6F_5$)); 109.4 (Cp); 60.8, 28.7 (*t*-Bu); 9.2 (br. Me–B); C≡NCMe$_3$ not observed. Anal. calc. for $C_{39}H_{27}BF_{15}HfN$ (989.9): C 47.61, H 2.77, N 1.56; found: C 47.38, H 2.82, N 1.52.

*X-Ray Crystal-Structure Analysis of* **9a**·*[B(C$_6$F$_5$)(Me)]*$^-$ [5]). Formula $C_{39}H_{27}BF_{15}HfN$, *M* 983.92; 0.60 × 0.50 × 0.20 mm; $a = 13.299(1)$, $b = 13.146(1)$, $c = 21.046(2)$ Å, $\beta = 100.49(1)°$, $V = 3617.9(5)$ Å$^3$, $\rho_{calc} = 1.806$ g cm$^{-3}$; $\mu = 29.92$ cm$^{-1}$; empirical absorption correction *via* $\varphi$ scan data ($0.782 \le C \le 0.999$); $Z = 4$, monoclinic, space group $P2_1/n$ (No. 14); $\lambda = 0.71073$ Å, $T$ 223 K, $\omega/2\theta$ scans, 7664 reflections collected ($+h$, $+k$, $\pm l$), $(\sin\theta)/\lambda = 0.62$ Å$^{-1}$, 7342 independent and 5824 observed reflections ($I \ge 2\sigma(I)$), 518 refined parameters; $R = 0.024$, $wR^2 = 0.055$; max. residual electron density 0.60 (– 0.79) e Å$^{-3}$, H-atoms calculated and refined as riding atoms.

*Carbonyltris(η$^5$-cyclopentadienyl)hafnium(1+) Methyltris(pentafluorophenyl)borate(1–)* (**9b**·[$B(C_6F_5)_3(Me)]^-$). To a mixture of **7c** (100 mg, 257 μmol) and $B(C_6F_5)_3$ (171 mg, 334 μmol) was added $CH_2Cl_2$ (10 ml) at 0° in a CO atmosphere. The mixture was stirred for 10 min under CO at 0° and then cooled to $-30°$ to crystallize the product which was obtained as single crystals suited for the X-ray crystal-structure analysis: 77 mg (32%) of **9b**. M.p. 55° (with CO cleavage). IR (KBr): 3123, 2971, 2940, 2137, 1643, 1513, 1268, 1089, 952, 804. $^1$H-NMR ($CD_2Cl_2$, 600 MHz, 243 K): 5.94 (*s*, 3 Cp); 0.42 (br. *s*, Me–B). $^{13}$C-NMR ($CD_2Cl_2$, 150.9 MHz, 243 K): 201.0 (CO), 110.4 (Cp). Anal. calc. for $C_{35}H_{18}BF_{15}HfO$ (928.8): C 45.26, H 1.95; found: C 44.25, H 2.14.

*X-Ray Crystal-Structure Analysis of* **9b**·*[B(C$_6$F$_5$)$_3$(Me)]*$^-$ [5]). Formula $C_{35}H_{18}BF_{15}HfO \cdot CH_2Cl_2$, *M* 1013.72; 0.30 × 0.30 × 0.20 mm; $a = 12.528(1)$, $b = 14.989(2)$, $c = 18.402(1)$ Å, $V = 3455.6(6)$ Å$^3$, $\rho_{calc} = 1.949$ g cm$^{-3}$; $\mu = 32.87$ cm$^{-1}$; empirical absorption correction *via* $\varphi$ scan data ($0.825 \le C \le 0.999$); $Z = 4$, orthorhombic, space group $P2_12_12_1$ (No. 19); $\lambda = 0.71073$ Å, $T$ 223 K, $\omega/2\theta$ scans, 3919 reflections collected ($+h$, $+k$, $\pm l$), $(\sin\theta)/\lambda = 0.62$ Å$^{-1}$, 3919 independent and 3143 observed reflections ($I \ge 2\sigma(I)$), 506 refined parameters; $R = 0.043$, $wR^2 = 0.095$; max. residual electron density 1.02 (– 2.14) e Å$^{-3}$ close to Hf, *Flack* parameter 0.02(4), H-atoms calculated and refined as riding atoms.

*Tris(η$^5$-cyclopentadienyl)methyltitanium* (**7a**). A soln. of [TiCl(Cp)$_2$(Me)] (**6a**; 1.44 g, 6.28 mmol) in toluene (50 ml) was added to a suspension of sodium cyclopentadienide (0.74 g, 8.37 mmol) in toluene (30 ml). The mixture was stirred overnight and filtered. The clear filtrate was concentrated *in vacuo* to *ca.* 30 ml. Pentane was added to precipitate the product that was collected by filtration, washed with pentane, and dried *in vacuo*; a second fraction of the product was obtained from the mother liquor: 1.05 (65%) of **7a**. M.p. 80°. The very sensitive product was characterized spectroscopically. IR (KBr): 3089, 2956, 2885, 1442, 1016, 806. $^1$H-NMR ($CD_2Cl_2$, 200 MHz): at 263 K: 5.86 (br. *s*, 3 Cp); 0.33 (*s*, Me); at 243 K: 5.89 (*s*, 2Cp); 5.70 (*s*, 1Cp). $^1$H-NMR ((D$_8$)toluene, 200 MHz): at 273 K: 5.38 (*s*, 3 Cp); 0.21 (*s*, Me); at 253 K: 5.87 (*s*, 1 Cp); 5.28 (*s*, 2 Cp); 0.23 (*s*, Me). $^{13}$C-NMR ($CD_2Cl_2$, 150 MHz): 116.2 (Cp); 49.5 (Me).

*Generation of Tris(cyclopentadienyl)titanium(1+) Methyltris(pentafluorophenyl)borate(1–)* (**10**·[$B(C_6F_5)_3(Me)]^-$). A soln. of [Ti(Cp)$_3$(Me)] (10.0 mg, 38.7 μmol) was treated with $B(C_6F_5)_3$ (21 mg, 41 μmol) in freshly condensed $CDFCl_2$ at $-78°$. The resulting product **10**·[$B(C_6F_5)_3(Me)]^-$ was directly characterized by temperature-dependent $^1$H-NMR (600 MHz) between 143 and 213 K. $^1$H-NMR ($CDFCl_2$, 600 MHz): at 143 K: 7.80 (br. *s*, 2 H); 6.89 (br. *s*, 2 H), 6.34 (br. *s*, 1 H, $\eta^2$-Cp); 7.06 (*s*, 5 H, $\eta^5$-Cp); 6.70 (*s*, 5 H, $\eta^5$-Cp); 0.30 (br. *s.*, 3 H, Me–B); at 213 K: 6.96 (br. *s*, 15 H, Cp); 0.35 (br., 3 H, Me–B).

3. *Computational Methods. General Procedure.* All calculations were based on the local-density approximation (LDA) in the parametrization of *Vosko et al.* [27], with the addition of gradient corrections due to *Becke* [28] and *Perdew* [29] (GGA). The GGA was included self-consistently (NL-SCF). The calculations utilized the Amsterdam Density Functional package ADF [30], release 2.0.1. Use was made of the frozen-core approximation. For C, the valence shell was described using a double ζ-STO basis, augmented by

---

[5]) The data sets were collected with an *Enraf Nonius Mach3* diffractometer. Programs used: data reduction MolEN, structure solution SHELXS-86, structure refinement SHELXL-93, graphics DIAMOND. Crystallographic data (excluding structure factors) for the structures reported in this paper have been deposited with the *Cambridge Crystallographic Data Centre* as supplementary publication No. CCDC-101305. Copies of the data can be obtained free of charge on application to The Director, CCDC, 12 Union Road, Cambridge CB2 1EZ, UK (fax: int. code +44(1223)336-033; e-mail: deposit@ccdc.cam.ac.uk).

one *d*-STO polarization function (ADF database III). For the *n*s, *n*p, *n*d, $(n+1)$s, and $(n+1)$p shells on Ti, Zr, and Hf, a triple $\zeta$-STO basis was employed (derived from ADF database IV). H was treated with a double $\zeta$-STO basis and one additional *p*-STO polarization function (ADF database III). The numerical integration grid was chosen in a way that significant test integrals are evaluated with an accuracy of at least four significant digits. For Hf, relativistic effects were included using a quasi-relativistic approach [31]. For systems with an odd electron count, spin-unrestricted calculations were performed.

*Energy Decomposition*. The *Hohenberg-Kohn* theory implies that the energy $E$ of a given system is a functional of the ground-state density $\rho$. In addition, there exists a ground-state wave function $\Psi_0$, which also is a functional of $\rho$ [32]. We thus can write *Eqn. 5* where $H_{KS}$ is the corresponding *Kohn-Sham* operator [33]. *Eqn. 5* holds for any density, real or fictive, and this fact is utilized in our energy analysis.

$$E[\rho] = \langle \Psi_0[\rho] \,|\, \hat{H}_{KS} \,|\, \Psi_0[\rho] \rangle \tag{5}$$

Given a molecule AB consisting of two single fragments A and B, the densities associated with the fragments are $\rho_A$ and $\rho_B$, with the corresponding wavefunctions $\Psi_A[\rho_A]$ and $\Psi_B[\rho_B]$ and fragment energies $E_A[\rho_A]$ and $E_B[\rho_B]$. For the sake of simplicity, we now drop the indication of the functional dependency between energy and density or wavefunction and density. When forming the molecule, we first construct a pre-molecule by superposition of the fragments in their position of the final molecule. Its density $\rho_{AB}$ is a superposition of the fragment densities, and the associated wavefunction $\Psi^0_{AB}$ is just the product $\Psi_A\Psi_B$, suitably antisymmetrized and normalized (*Eqn. 6*). The total energy $E^0$ of this system is given by *Eqn. 7*, and the contribution to the bonding energy, $\Delta E^0$, by *Eqn. 8* where $\hat{H}_A$, $\hat{H}_B$, and $\hat{H}_{AB}$ are the corresponding *Kohn-Sham* operators of the fragments and the molecule. As mentioned before, the steric repulsion term $\Delta E^0$ can be broken down into electrostatic interaction $\Delta E_{elstat}$ and *Pauli* repulsion $\Delta E_{Pauli}$ [34], according to *Eqn. 2*. In particular, $\Delta E_{elstat}$ is given by *Eqn. 9*. $\Delta E_{Pauli}$ is then the remaining contribution to $\Delta E^0$. The third term which determines the bonding energy $BE$ as defined in *Eqn. 1* is the interaction energy $\Delta E_{int}$. It is associated with the change in density on going from the superposition of the fragment densities $\rho_{AB}$ to the density of the final molecule $\rho_{(AB)}$, and might be written as *Eqn. 10* [35]

$$\Psi^0_{AB} = N\mathcal{A}[\Psi_A\Psi_B] \tag{6}$$

$$E^0 = \langle \Psi^0_{AB} \,|\, \hat{H}_{AB} \,|\, \Psi^0_{AB} \rangle \tag{7}$$

$$E^0 = \langle \Psi^0_{AB} \,|\, \hat{H}_{AB} \,|\, \Psi^0_{AB} \rangle - \langle \Psi_A \,|\, \hat{H}_A \,|\, \Psi_A \rangle - \langle \Psi_B \,|\, \hat{H}_B \,|\, \Psi_B \rangle \tag{8}$$

$$\Delta E_{elstat} = \frac{Z_A Z_B}{R} + \int \frac{\rho_A(1)\rho_B(2)}{|r_1 - r_2|} dr_1 dr_2 + \int \rho_A(1) V^B_N dr_1 + \int \rho_B(1) V^A_N dr_1 \tag{9}$$

$$\Delta E_{int} = \int_{E^0[\rho_{AB}]}^{E[\rho_{AB}]} \mathrm{d}E \tag{10}$$

## REFERENCES


[1] R. D. Rogers, R. V. Bynum, J. L. Atwood, *J. Am. Chem. Soc.* **1978**, *100*, 5238; see also V. I. Kulishov, E. M. Brainina, N. G. Bokiy, Yu. T. Struchkov, *J. Chem. Soc., Chem. Commun.* **1970**, 475.

[2] J. W. Lauher, R. Hoffmann, *J. Am. Chem. Soc.* **1976**, *98*, 1729.

[3] B. E. Bursten, L. F. Rhodes, R. J. Strittmatter, *J. Am. Chem. Soc.* **1989**, *111*, 2756, 2758.

[4] J. L. Calderon, F. A. Cotton, B. G. DeBoer, J. Takats, *J. Am. Chem. Soc.* **1971**, *93*, 3592.

[5] R. D. Rogers, R. V. Bynum, J. L. Atwood, *J. Am. Chem. Soc.* **1981**, *103*, 692.

[6] B. V. Lokshin, Z. S. Klemenkova, M. G. Ezernitskaya, L. I. Strunkina, E. M. Brainina, *J. Organomet. Chem.* **1982**, *235*, 69; see also E. M. Brainina, L. I. Strunkina, B. V. Lokshin, M. G. Ezernitskaya, *Izv. Akad. Nauk. SSSR, Ser. Khim.* **1981**, 447; E. M. Brainina, L. I. Strunkina, *ibid.* **1983**, 2160.

[7] W. W. Lukens, Jr., R. A. Andersen, *Organometallics* **1995**, *14*, 3435.

[8] M. M. Corradi, D. J. Duncalf, G. A. Lawless, M. P. Waugh, *J. Chem. Soc., Chem. Commun.* **1997**, 203.

[9] C. R. Lucas, M. Green, R. A. Forder, K. Prout, *J. Chem. Soc., Chem. Commun.* **1973**, 97.

[10] a) T. Brackemeyer, G. Erker, R. Fröhlich, *Organometallics* **1997**, *16*, 531; b) T. Brackemeyer, G. Erker, R. Fröhlich, J. Prigge, U. Peuchert, *Chem. Ber.* **1997**, *130*, 899.

[11] J. L. Atwood, K. D. Smith, *J. Am. Chem. Soc.* **1973**, *95*, 1488; M. Adam, U. Behrens, R. D. Fischer, *Acta Crystallogr., Sect. C* **1991**, *47*, 968; S. H. Eggers, J. Kopf, R. D. Fischer, *Organometallics* **1986**, *5*, 383; P. G. Laubereau, J. H. Burns, *Inorg. Chem.* **1970**, *9*, 1091; S. H. Eggers, W. Hinrichs, J. Kopf, W. Jahn, R. D. Fischer, *J. Organomet. Chem.* **1986**, *311*, 313; S. H. Eggers, J. Kopf, R. D. Fischer, *Acta Crystallogr., Sect. C* **1987**, *43*, 2288; for $[Tc(Cp)_3]$, the results of an X-ray analysis are interpreted as $2\eta^5\eta^1$ coordination: C. Apostolidis, B. Kanellakopulos, R. Maier, J. Rebizant, M. L. Ziegler, *J. Organomet. Chem.* **1991**, *411*, 171; see also J. D. Fisher, P. H. M. Budzelaar, P. J. Shapiro, R. J. Staples, G. P. A. Yap, A. L. Rheingold, *Organometallics* **1997**, *16*, 871.

[12] T. Ziegler, *Chem. Rev.* **1991**, *91*, 651. T. Ziegler, *Can. J. Chem.* **1995**, *73*, 743.

[13] E. J. Baerends, N. Rozendaal, *NATO Adv. Study Inst. Ser.* **1986**, *C176*, 159; T. Ziegler, *ibid*. **1991**, *C378*, 367.

[14] C. Sonntag, H. Berke, C. Sarter, G. Erker, *Helv. Chim. Acta* **1989**, *72*, 1676.

[15] P. Pyykkö, J.-P. Declaux, *Acc. Chem. Res.* **1979**, *12*, 276; P. Pyykkö, *Chem. Rev.* **1988**, *88*, 563; W. H. E. Schwarz, E. M. van Wezenbeck, E. J. Baerends, J. G. Snijders, *J. Phys. B: At. Mol. Opt. Phys.* **1989**, *22*, 1515.

[16] a) T. A. Albright, J. K. Burdett, M.-H. Whangboo, 'Orbital Interactions in Chemistry', John Wiley, New York, 1985, pp. 302; b) *ibid*., pp. 95; c) *ibid*. pp. 78.

[17] A. S. Goldman, K. Krogh-Jespersen, *J. Am. Chem. Soc.* **1996**, *118*, 12159.

[18] P. C. Wailes, H. Weigold, *J. Organomet. Chem.* **1970**, *24*, 405.

[19] J. R. Surtees, *J. Chem. Soc., Chem. Commun.* **1965**, 567.

[20] J. C. W. Chien, W. M. Tsai, M. D. Rausch, *J. Am. Chem. Soc.* **1991**, *113*, 8570.

[21] M. Bochmann, L. M. Wilson, M. B. Hursthouse, M. Motevalli, *Organometallics* **1988**, *7*, 1148; M. Bochmann, A. J. Jagger, J. C. Nicholls, *Angew. Chem.* **1990**, *102*, 830; *ibid.*, *Int. Ed. Engl.* **1990**, *29*, 780.

[22] a) F. G. A. Stone, A. G. Massey, A. J. Park, *Proc. Chem. Soc.* **1963**, 212; A. G. Massey, A. J. Park, *J. Organomet. Chem.* **1964**, *2*, 245; b) X. Yang, C. L. Stern, T. J. Marks, *J. Am. Chem. Soc.* **1991**, *113*, 3623; *ibid*. **1994**, *116*, 10015.

[23] Z. Guo, D. C. Swenson, A. S. Guram, R. F. Jordan, *Organometallics* **1994**, *13*, 766, and ref. cit. therein; see also P. K. Hurlburt, J. J. Rack, J. S. Luck, S. F. Dec, J. D. Webb, O. P. Anderson, S. H. Strauss, *J. Am. Chem. Soc*. **1994**, *116*, 10003; B. Temme, G. Erker, J. Karl, H. Luftmann, R. Fröhlich, S. Kotila, *Angew. Chem.* **1995**, *107*, 1867; *ibid*., *Int. Ed. Engl*. **1995**, *34*, 1755; D. M. Antonelli, E. B. Tjaden, J. M. Stryker, *Organometallics* **1994**, *13*, 763; A. S. Guram, D. C. Swenson, R. F. Jordan, *J. Am. Chem. Soc.* **1992**, *114*, 8991.

[24] For related examples, see *e.g.* J. Köpf, H.-J. Vollmer, W. Kaminsky, *Cryst. Struct. Commun*. **1980**, *9*, 985; H.-J. Sinn, W. Kaminsky, H.-J. Vollmer, R. Woldt, *Angew. Chem.* **1980**, *92*, 396; *ibid., Int. Ed. Engl*. **1980**, *19*, 390.

[25] F. H. Allen, O. Kennard, D. G. Watson, L. Brammer, A. G. Orpen, R. Taylor, *J. Chem. Soc., Perkin Trans. 2* **1987**, S1.

[26] E. M. Brainina, G. G. Dvoryantseva, *Izv. Akad. Nauk SSSR, Ser. Khim.* **1967**, 442; J. L. Calderon, F. A. Cotton, J. Takats, *J. Am. Chem. Soc*. **1971**, *93*, 3587; E. M. Brainina, N. P. Gambaryan, B. V. Lokshin, P. V. Petrovskii, Yu. T. Struchkov, E. N. Kharlamova, *Izv. Akad. Nauk SSSR, Ser. Khim*. **1972**, 187; L. M. Hansen, D. S. Marynick, *J. Am. Chem. Soc.* **1988**, *110*, 2358; *Organometallics* **1989**, *8*, 2173; R. J. Strittmatter, B. E. Bursten, *J. Am. Chem. Soc*. **1991**, *113*, 552.

[27] S. J. Vosko, M. Wilk, M. Nussair, *Can. J. Phys.* **1980**, *58*, 1200.

[28] A. D. Becke, *J. Chem. Phys.* **1986**, *84*, 4524; *ibid*. **1988**, *88*, 1053; *Phys. Rev. A* **1988**, *38*, 3098.

[29] J. P. Perdew, *Phys. Rev. B: Condens. Matter* **1986**, *33*, 8822; *ibid.* **1986**, *34*, 7406.

[30] E. J. Baerends, D. E. Ellis, P. E. Ros, *Chem. Phys.* **1973**, *2*, 41; G. teVelde, E. J. Baerends, *J. Comp. Phys.* **1992**, *99*, 84; C. Fonseca Guera, O. Visser, J. G. Snijders, G. Te Velde, E. J. Baerends, in 'Methods and Techniques in Computational Chemistry: METECC-95', Eds. E. Clementi and G. Corongiu, STEF, Cagliari, 1995, p. 305. G. teVelde, 'ADF 2.1 User's Guide', Vrije Universiteit, Amsterdam, 1996.

[31] T. Ziegler, V. Tschinke, E. J. Baerends, J. G. Snijders, W. Ravenek, *J. Phys. Chem.* **1989**, *93*, 3050; G. Schreckenbach, J. Li, T. Ziegler *Int. J. Quantum Chem.* **1995**, *56*, 477.

[32] E. J. Baerends, O. V. Gritsenko *J. Phys. Chem. A* **1997**, *101*, 5383.

[33] R. G. Parr, W. Yang, 'Density Functional Theory of Atoms and Molecules', Oxford University Press, Oxford, 1989.

[34] P. J. van den Hoeck, A. W. Kleyn, E. J. Baerends *Comments At. Mol. Phys.* **1989**, *23*, 93.

[35] T. Ziegler, A. Rauk, *Theor. Chim. Acta* **1977**, *46*. 1.

*Received April 15, 1998*